ACS Catalysis

Research Article

Cite This: ACS Catal. 2019, 9, 1739−1747

pubs.acs.org/acscatalysis

Structural Insights into the Dual-Substrate Recognition and Catalytic Mechanisms of a Bifunctional Acetyl Ester−Xyloside Hydrolase from *Caldicellulosiruptor lactoaceticus*

Hao Cao,[†,▽] Lichao Sun,[†,▽] Ying Huang,[†] Xin Liu,[†,‡] Dong Yang,[§] Tengfei Liu,[∥] Xiaojing Jia,[⊥,#] Boting Wen,[†] Tianyi Gu,[†] Fengzhong Wang,[*,†] and Fengjiao Xin[*,†]

[†]Laboratory of Biomanufacturing and Food Engineering, Institute of Food Science and Technology, Chinese Academy of Agricultural Sciences, Beijing 100193, China

[‡]Hefei National Laboratory for Physical Sciences at Microscale, School of Life Sciences, University of Science and Technology of China, Hefei 230027, China

[§]College of Food Science and Nutritional Engineering, China Agricultural University, Beijing 100083, China

[∥]School of Chinese Materia Medica, Beijing University of Chinese Medicine, Beijing 100102, China

[⊥]National Key Laboratory of Biochemical Engineering, Institute of Process Engineering, Chinese Academy of Sciences, Beijing 100190, China

[#]University of Chinese Academy of Sciences, Beijing 100049, China

Supporting Information

ABSTRACT: Enzymes are usually characterized by their evolutionarily conserved catalytic domains; however, this work presents the incidental gain-of-function of an enzyme in a loop region by natural evolution of its amino acids. A bifunctional acetyl ester−xyloside hydrolase (CLH10) was heterologously expressed, purified, and characterized. The primary sequence of CLH10 contains the fragments of the conserved sequence of esterase and glycosidase, which distribute in a mixed type. The crystal structure revealed that the primary sequence folded into two independent structural regions to undertake both acetyl esterase and β-1,4-xylanase hydrolase functions. CLH10 is capable of cleaving both the β-1,4-xylosidic bond-linked main chain and the ester bond-linked acetylated side chain of xylan, which renders it valuable because it can degrade acetylated xylan within one enzyme. Significantly, the β-1,4-xylanase activity of CLH10 appears to have been fortuitously obtained because of the variable Asp10 and Glu139 located in its loop region, which suggested that the exposed loop region might act as a potential hot-spot for the design and generation of promising enzyme function in both directed evolution and rational protein design.

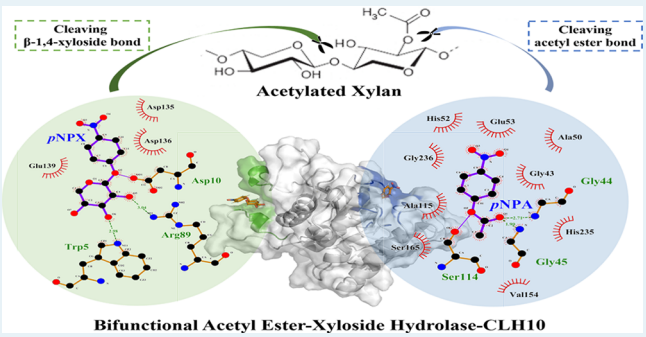

KEYWORDS: *bifunctional hydrolase, acetyl esterase, β-1,4-xylanase, dual-substrate, catalytic mechanisms*

1. INTRODUCTION

In contrast to monofunctional enzymes, bifunctional enzymes can catalyze different types of reactions, which reduces the number of enzyme types needed and decreases the cost of bioengineering processes.[1,2] Natural evolution developed a class of bifunctional enzymes that addresses the complicated binding within xylan, including bifunctional xyloside−xyloside hydrolase,[3] bifunctional arabinoside−xyloside hydrolase[4] and bifunctional acetyl ester−xyloside hydrolase.[5]

Various types of xylans and other hemicelluloses are often acetylated in natural environments. Hence, both carboxylesterase and glycoside hydrolases are expected to be used in the enzymatic degradation of acetyl xylan to deacetylate xylan and cleave the xylosidic bond, respectively.[6,7] Carboxylesterase (EC 3.1.1) activity is often based on a conserved catalytic triad (Asp/Glu−His−Ser),[8] while the activity of glycoside hydrolases (EC 3.2.1) usually involves a retaining or inverting mechanism based on a conserved catalytic amino acid pair (Asp/Glu−Asp/Glu).[9] Bifunctional acetyl ester−xyloside hydrolase (AEXH) has the catalytic properties of both carboxylesterase and glycoside hydrolase simultaneously. In some cases, AEXHs contain two separate sequence regions (SRs) within a single polypeptide, which represent two individual catalytic domains to hydrolyze ester bonds and xylosidic bonds, respectively.[2]

Received: August 23, 2018
Revised: January 10, 2019
Published: January 14, 2019

Downloaded via CHINESE ACADEMY AGRICULTURAL SCI on October 17, 2019 at 00:45:10 (UTC).
See https://pubs.acs.org/sharingguidelines for options on how to legitimately share published articles.

© 2019 American Chemical Society

DOI: 10.1021/acscatal.8b03383
ACS Catal. 2019, 9, 1739−1747

Caldicellulosiruptor lactoaceticus (*C. lactoaceticus*) 6A can utilize natural xylan as its carbon source.[10] Unusually, the primary sequence of a thermophilic hydrolase from *C. lactoaceticus* (CLH10) contains the fragments of the conserved sequence of esterase (CSE) and the conserved sequence of glycosidase (CSG), which distribute in a mixed type. CLH10 was shown to hydrolyze both β-1,4-xylosidic bonds and acetyl ester bonds in the enzymatic activity assays, indicating that CLH10 is a typical AEXH and is valuable for the enzymatic degradation of xylan. The crystal structure of apo-CLH10 was solved to investigate the atomic basis of the structure−bifunction relationship. Molecular dockings and mutational studies verified the dual-substrate recognition and catalytic mechanisms of CLH10. This work revealed how CLH10 performs two distinct functionalities through natural evolution of its amino acids within the specific fold of one structural domain.

2. EXPERIMENTAL SECTION

2.1. Strains, Plasmids, And Chemicals. Competent cells, namely, *Escherichia coli* DH5a and BL21-Gold (*DE3*) (TransGen Biotech China), were used as hosts for plasmid amplification and protein expression, respectively. The DNA sequence encoding CLH10 (*CHL10*) was inserted into plasmid pET28b (+) (Novagen) between the *Nde*I and *Xho*I restriction nuclease sites, and the His_6-tag encoding sequence was positioned in-frame in front of *CHL10*. *p*-Nitrophenyl-β-D-xylopyranoside (*p*NPX) and *p*-nitrophenyl acetate (*p*NPA) were purchased from Aladdin Co., Ltd. All chemicals were of analytical grade or higher quality.

2.2. Construction of the Site-Directed Mutants. Site-directed mutants of CLH10 were constructed with a quick-change site-directed mutagenesis kit (TaKaRa). The primers are shown in Table S1.

2.3. Heterologous Expression and Purification. The expression and purification of CLH10 and its mutants were carried out by the same protocol described in our previous work.[11] The purified CLH10 (Figure S1) and its mutants were concentrated and stored at −80 °C.

2.4. Protein Crystallization, X-ray Data Collection, And Structure Determination. The screening of crystallization conditions was carried out according to the same methods described by our previous work except that the drop volume was 2 μL containing 1 μL of protein sample (4.9 mg/mL) and 1 μL of reservoir solution.[11] The optimized crystallization buffer consisted of 0.8 M potassium phosphate, pH 7.5. The selected crystals were mounted in cryoloops, passed through the cryoprotectant solution consisting of 25% ethylene glycol (v/v) and 0.4 M potassium phosphate, and flash-frozen in liquid nitrogen. The X-ray diffraction data set was collected from a single crystal using a frame width of 1° and oscillation range of 360° at Shanghai Synchrotron Radiation Facility (SSRF) beamline BL19U1 (Shanghai, China), equipped with a Pilatus 6 M detector. The HKL3000 package was employed to process the collected data.[12] ARP/wARP,[13] CCP4,[14] PHENIX,[15] and Coot[16] packages were employed to build and refine the structure of CLH10 using the molecular replacement strategy, in which the published crystal structure (PDB: 3HXK) was used as a template. The refined coordinates and structure factors of CLH10 were deposited in the Protein Data Bank with the accession code 6A6O.[17]

2.5. Enzymatic Activity Assay. The hydrolysis of the β-1,4-xylosidic bond and acetyl ester bond was measured based on a photometric assay of the released *p*-nitrophenol detected at 410 nm in a microtiter plate (MTP) using *p*NPX and *p*NPA as substrates, respectively.

The reaction mixture in each well of the MTP was prepared by adding 10 μL of enzyme solution to 90 μL of buffer. The MTP was then incubated for 10 min. Subsequently, 100 μL of the precooled substrate solution (1 mM) was added, and the absorbance value was measured after incubation. One unit (U) of enzyme activity was defined as the amount of enzyme releasing 1 μmol of *p*-nitrophenol per minute under the assay conditions.

2.6. Optimal pH for Enzymatic Activity. For an investigation of the effect of pH on the esterase activity of CLH10, following the above enzymatic activity assay, the reaction mixture in each well of the MTP was prepared by adding 10 μL of enzyme solution to 90 μL of different buffers, which covered a pH range 6.0−10.0 using citrate buffer (pH 3.0−6.0), sodium phosphate buffer (pH 6.0−7.0), Tris−HCl buffer (pH 7.0−8.0), and NaOH−glycine buffer (pH 8.0−9.0). The same procedure was carried out to examine the effect of pH on the β-1,4-xylanase activity of CLH10.

2.7. Optimal Temperature for Enzymatic Activity. For an investigation of the effect of temperature on the esterase activity of CLH10, the reaction mixture in the MTP was incubated at different test temperatures (30−100 °C with 5 °C intervals) for 10 min. Subsequently, precooled substrate solution (1 mM) was added. The same procedure was carried out to examine the effect of temperature on the β-1,4-xylanase activity of CLH10.

2.8. Kinetic Parameters. Steady-state kinetic measurements were performed at the optimal temperature and pH for the esterase activity and β-1,4-xylanase of CLH10 by varying the concentrations (0.125−10 mM) of *p*NPX and *p*NPA, respectively. The K_m and k_{cat} values were calculated from the initial rate of *p*-nitrophenol liberation. Protein concentration was assayed with a DC protein assay kit (Bio-Rad) by using bovine serum albumin as a standard. The reaction mixture with the denatured enzyme solution was taken as the blank group, and all data are shown as averages with the standard deviation (n = 3).

2.9. Cooperative Effect of Dual-Substrate on Enzymatic Activity. Xylotetraose (5% w/v) and *p*NPA (1 mM) were separately and simultaneously added to the unary-substrate and dual-substrate reaction systems, respectively. Hydrolysis reactions with the enzyme (0.49 mg/mL) were performed at 65 °C, pH 6.5. The amount of *p*-nitrophenol released was measured by its absorbance at 410 nm. The amount of reducing sugars released from xylotetraose was measured using the 3,5-dinitrosalicylic acid (DNS) method.[18] The reaction mixture with the denatured enzyme solution was taken as the blank group, and all data are shown as averages with the standard deviation (n = 3).

2.10. Computational Procedures. Evolutionary conservation analysis of sequences was performed using the ConSurf Web site server (http://consurf.tau.ac.il) to identify related sequences in the UniRef90 database.[19−21] The Basic Local Alignment Search Tool (BLAST) with the accelerated protein−protein BLAST algorithm was used to search and align the target sequence.[22] DNAMAN software was used to align and show the extracted reference sequences.

DOI: 10.1021/acscatal.8b03383
ACS Catal. 2019, 9, 1739−1747

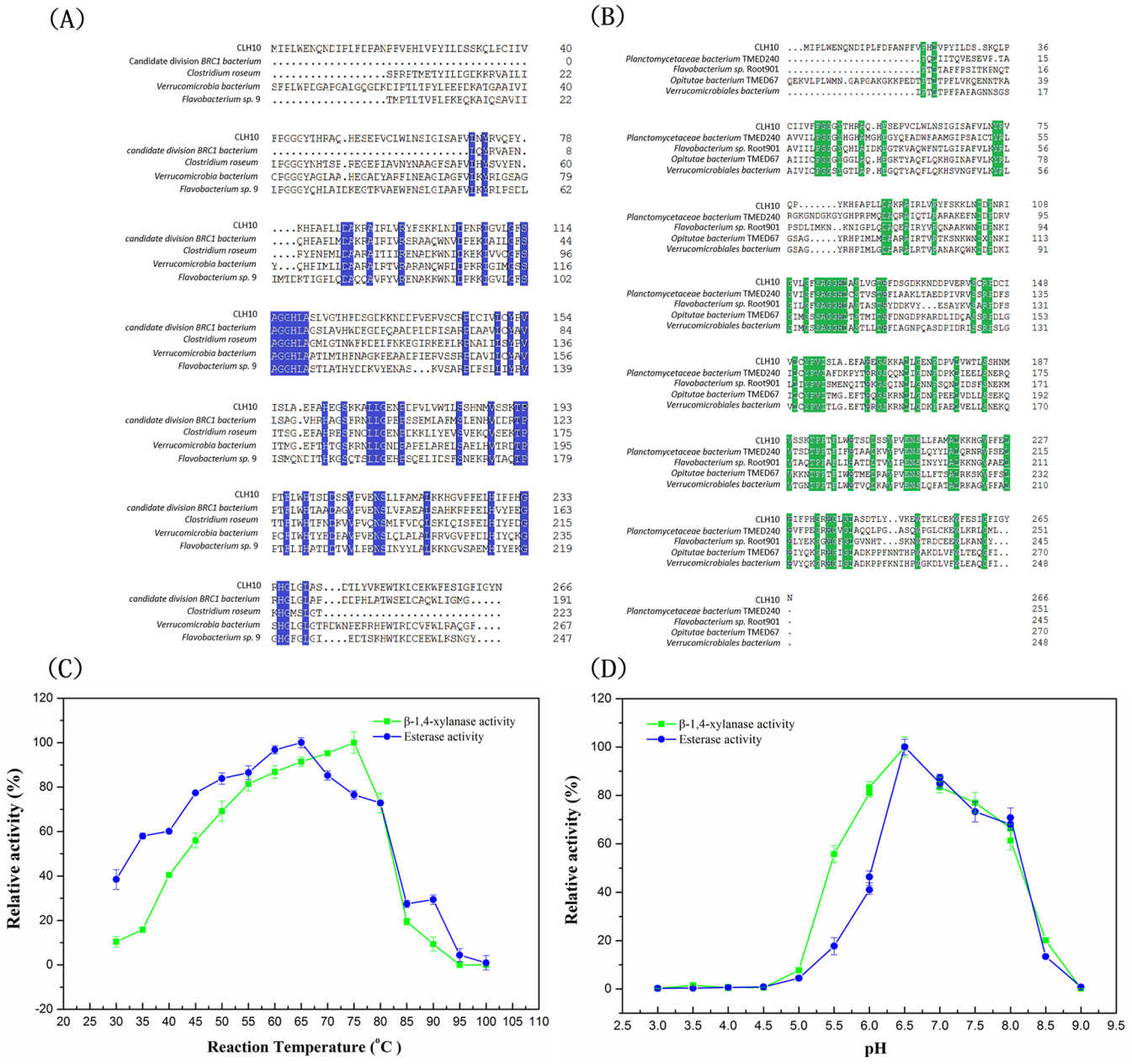

Figure 1. Acetyl ester and xyloside hydrolysis activity of CLH10. (A) Sequence alignment of CLH10 and the referenced acetyl esterases. (B) Sequence alignment of CLH10 and the referenced β-1,4-xylanases. (C) Effect of temperature on acetyl esterase and β-1,4-xylanase activity. The acetyl esterase activity at 65 °C is set as 100% (407.7 U/mg), and the β-1,4-xylanase activity at 75 °C is set as 100% (8.93 U/mg). (D) Effect of pH on the acetyl esterase and β-1,4-xylanase activity. The acetyl esterase activity at pH 6.5 is set as 100% (438.6 U/mg); the β-1,4-xylanase activity at pH 6.5 is likewise set as 100% (10.21 U/mg).

Molecular docking was performed with the YASARA software package using the Autodock Vina algorithm.[23,24] Water molecules were stripped from the receptor, and hydrogen atoms were added for the receptor before molecular docking. Ligand conformation was pretreated by the semi-empirical quantum mechanics (MOPAC).[25] First, 25 docking runs were performed for each molecular docking operation using the dock_run macro with the default parameters. Second, cluster analysis was carried out using the dock_play macro with the default parameters, which provides an interactive player for docking poses and clusters. After clustering of the above 25 runs, 3−6 distinct complex conformations were found and ranked according to their binding energy and dissociation constant. According to the evaluation of YASARA, more positive binding energies and smaller dissociation constants indicated better binding relationships between the receptor and ligand. As a result, the best-ranked ligand conformation in rank was viewed and analyzed by using the PyMOL package.[26]

Molecular dynamics simulations were performed with the YASARA software package using the AMBER11 force field (ff99SB).[27,28] The protein was embedded in a cubic box with a 1.0 nm space left around the protein for adding the water (TIP3P) system. The protein−solvent systems were simulated at 338 K and atmospheric pressure for 10 ns using the md_run macro. To reduce the bias of the initial atom velocities, three

DOI: 10.1021/acscatal.8b03383
ACS Catal. 2019, 9, 1739−1747

Location	Substitution	Substrate	K_m (mM)	k_{cat} (s^{-1})
Putative acetyl ester active region	Wild Type	*p*NPA	0.14±0.02	19.80±1.51
	S114A		N.D.	N.D.
	D203A		N.D.	N.D.
	H235A		N.D.	N.D.
	G44A		0.17±0.01	2.90±0.23
	G45A		0.18±0.01	2.03±0.14
Putative β-1,4-xylanase active region I	Wild Type	*p*NPX	26.77±1.21	0.53±0.02
	W5A		N.D.	N.D.
	W5F		26.21±0.92	0.48±0.02
	W5Y		37.44±0.84	0.48±0.03
	E6A		27.73±1.06	0.45±0.03
	D10A		N.D.	N.D.
	R89A		152.53±2.57	0.52±0.02
	D135A		6.75±0.24	0.91±0.03
	D135E		26.54±0.78	0.55±0.01
	D135N		N.D.	N.D.
	D136A		74.82±2.20	0.51±0.01
	E139A		N.D.	N.D.
Putative β-1,4-xylanase active region II	Wild Type	*p*NPX	26.77±1.21	0.53±0.02
	E53A		26.91±1.11	0.50±0.01
	D203A		27.18±0.74	0.51±0.01

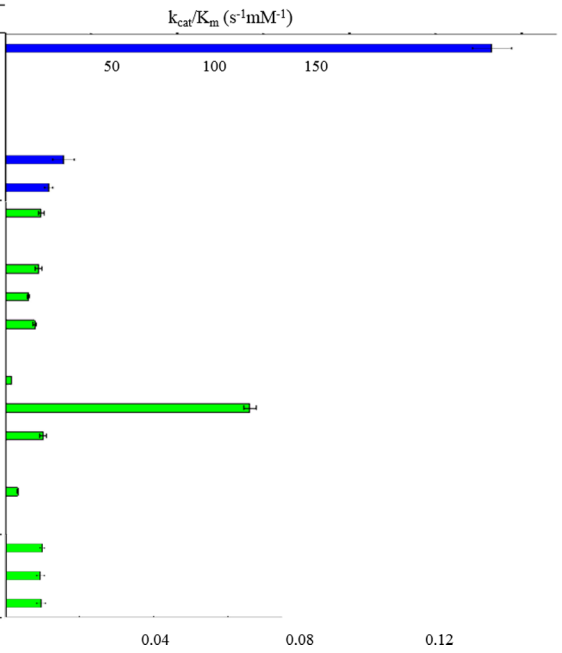

Figure 2. Kinetic parameters of CLH10 and its mutants in the hydrolysis of *p*NPA and *p*NPX.

independent MD simulations were carried out. The dynamic cross-correlation matrix (DCCM) was analyzed by the md_analyze macro, and the average was taken.

3. RESULTS

3.1. Sequence Mining. The nucleotide sequence of CLH10 is of 801 bp (accession number: WP014043093) and encodes a 267 amino acid protein annotated as the α/β hydrolase. CLH10 has high sequence similarity with the acetyl esterase from candidate division BRC1 *bacterium* (36.8%), *Clostridium roseum* (37.6%), *Verrucomicrobia bacterium* (41.9%), and *Flavobacterium sp.* 9 (40.8%) (Figure 1A). Furthermore, CLH10 contains the G-X-S-X-G consensus motif, which is characteristic of the active site of a serine hydrolase. On the other hand, the sequence of CLH10 is also highly similar to that of β-1,4-xylanase from *Planctomycetaceae bacterium* TMED240 (39.4%), *Flavobacterium sp.* Root 901 (39.0%), *Opitutae bacterium* TMED67 (46.1%), and *Verrucomicrobiales bacterium* (42.2%) (Figure 1B). The amino acid sequence alignment with the reference sequences implied that CLH10 was a putative bifunctional enzyme with both carboxylesterase activity and glycoside hydrolase activity.

3.2. Enzyme Activity Characterization. The finding that CLH10 was able to hydrolyze *p*NPA demonstrated that CLH10 was an acetyl esterase (Figure 1C). The optimal catalytic temperature of CLH10 was 65 °C. The activity sharply dropped at 80 °C, and the enzyme was almost inactivated at 95 °C. CLH10 activity was optimal at pH 6.5 and retained more than 70% of its relative activity in the pH range from 6.5 to 8.0. Additionally, CLH10 exhibited β-1,4-xylanase activity, as demonstrated by its hydrolysis against *p*NPX. As shown in Figure 1C, the activity of CLH10 was highest at 75 °C and decreased sharply at higher temperatures. In the activity assay at different pH values, pH 6.5 was optimal for the hydrolysis of both *p*NPX and *p*NPA by CLH10 (Figure 1D). The fact that CLH10 could hydrolyze both the acetyl ester bond and the β-1,4-xylosidic bond in the activity assay indicated that CLH10 is an AEXH. Furthermore, under the optimal temperature and pH conditions, the acetyl esterase activity of CLH10 toward *p*NPA had a K_m of 0.14 ± 0.02 mM and k_{cat} of 19.80 ± 1.51 s^{-1}, while the β-1,4-xylanase activity of CLH10 toward *p*NPX had a K_m of 26.77 ± 1.21 mM and k_{cat} of 0.53 ± 0.02 s^{-1} (Figure 2).

3.3. Determination of the Dual-Substrate Recognition and Catalytic Regions. The crystal structure of apo-CLH10 was solved and refined to 1.80 Å resolution (Table S2). The crystal contains one molecule per asymmetric unit, and the final model contains residues from Met1 to Gly264 of CLH10. The structure scaffold of CLH10 is highly similar to that of α/β hydrolase, in which seven β-strands are sandwiched by 10 α-helices (Figure 3A,B).

For the identification of the potential functional regions of CLH10 toward acetyl ester, the structure of CLH10 was employed to carry out the molecular dockings (Table S3). As shown in Figure 3B, the *p*NPA molecule docked into a target pocket that was a potential recognition and catalytic region for acetyl ester. The above sequence alignment results implied that Ser114 of CLH10 in the G-X-S-X-G consensus motif was a putative catalytic residue, acting as a nucleophile for the hydrolysis of the ester linkage. The catalytic mechanism of the catalytic triad suggested an electron rearrangement in the form Asp^{-} His Ser → Asp His Ser^{-} to increase the nucleophilicity of Ser.[29] In the present work, the acetyl ester group of *p*NPA inserted into the potential recognition pocket and oriented near Ser114, indicating that the spatial relationship between enzyme and substrate was feasible for catalysis. According to the conformation of *p*NPA, Ser114, His235, and Asp203 appeared to compose the putative catalytic triad of esterase at the bottom of the target pocket. Essentially, the critical step of the hydrolysis reaction was that His235 acts as the general base to capture a proton from Ser114. Then, the side chain oxygen atom of the deprotonated Ser114 acts as the nucleophile to attack the carbonyl carbon atom of the acetyl ester of *p*NPA. Furthermore, three single-site mutations (S114A, H235A, and D203A) showed barely detectable activity toward *p*NPA, indicating that Ser114, His235, and Asp203 were the critical

DOI: 10.1021/acscatal.8b03383
ACS Catal. 2019, 9, 1739−1747

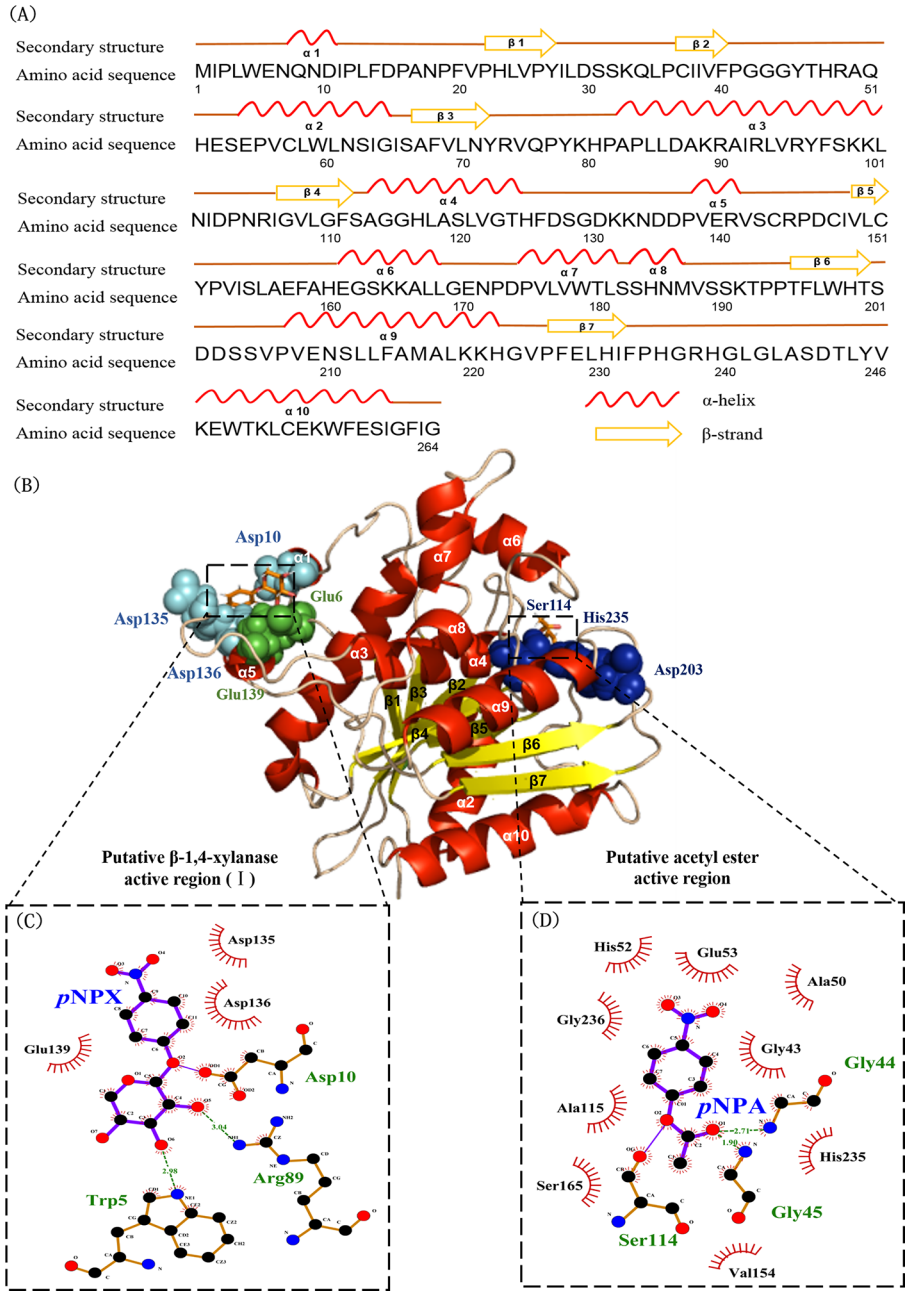

Figure 3. Dual-substrate recognition and catalytic regions of CLH10. (A) Alignment between the primary and secondary structure of CLH10. (B) Cartoon representation of CLH10. Wheat denotes the loop region, yellow denotes the β-sheet region, and red denotes the α-helix region. Ser114, Asp203, and His235 are shown as blue spheres. Asp10 135 and 136 and Glu6 139 are shown as cyan and green spheres, respectively. The *p*NPA and *p*NPX molecules are indicated as sticks in orange. LigPlot 2D diagram showing the detailed interaction of residues with *p*NPX (C) and *p*NPA (D). The model with solid circles and bold bonds represents the substrate docked in the protein. The model with solid circles and thin bonds depicts the amino acid residues of the active site of CLH10 forming hydrogen bonds or covalent bonds with the substrate; the dashed lines represent the putative hydrogen bonds, and the full lines represent the putative covalent bonds. The spokes pointing toward docked substrates represent hydrophobic interactions. Substrate atoms with spokes indicate that these atoms were involved in hydrophobic interactions.

catalytic residues of CLH10 toward acetyl ester hydrolysis (Figure 2).

Regarding the recognition and catalytic region of CLH10 toward the β-1,4-xylosidic bond, two complex conformations were filtered out considering the enzyme−substrate binding energy and distribution of potential catalytic residues (glutamate and aspartate) by molecular docking *in silico* (Tables S4 and S5). The β-1,4-xylanase requires either a two-step retaining or a single-step inverting catalytic mechanism, in which a catalytic pair composed of carboxylate residues, such as aspartate and glutamate (GH3 and GH43), glutamate and glutamate (GH30 and GH39), and glutamate and aspartate (GH52 and GH116), are critical to act as a nucleophile and general acid, respectively. One possible recognition and catalytic region (I) appeared to be an open carbohydrate-binding cleft that might allow accommodation of longer xylo-oligosaccharides than *p*NPX. Glu6, Asp10, Asp135, Asp136, and Glu139 were the potential catalytic residues, which were all located in this cleft (Figure 3B). Another possible recognition and catalytic region (II) was the same as the

DOI: 10.1021/acscatal.8b03383
ACS Catal. 2019, 9, 1739−1747

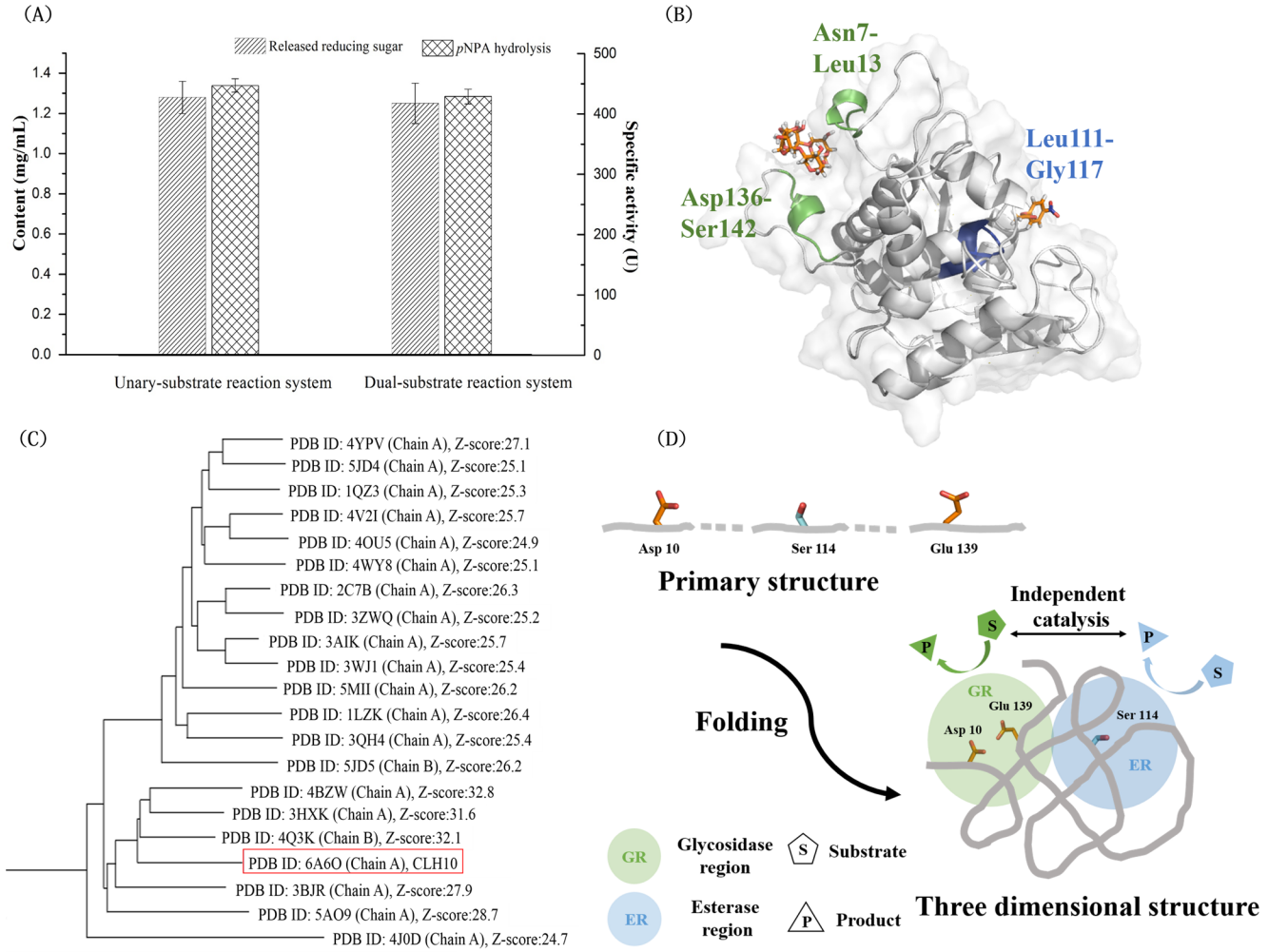

Figure 4. Relationship between the acetyl esterase and β-1,4-xylanase activity of CLH10. (A) Reducing sugar released from xylotetraose and specific activity toward *p*NPA hydrolysis in unary-substrate and dual-substrate systems. (B) Surface and cartoon representation of CLH10 with docking *p*NPA and xylotetraose. The residue region Leu111−Gly117 is given in blue, and the residue regions Asn7−Leu13 and Asp136−Ser142 are given in green. Both *p*NPA and xylotetraose molecules are indicated as sticks in orange. (C) Structural similarity dendrogram of CLH10. The dendrogram is derived by average linkage clustering of the structural similarity matrix by the DALI server. PDB IDs are provided by the Protein Data Bank. *Z*-scores are provided by the DALI server. (D) Sketch of bifunctional behavior of CLH10.

above recognition and catalytic pocket of CLH10 for acetyl ester. The potential catalytic pair (Glu53 and Asp203) located in this pocket could bind a xylose molecule in the appropriate spatial arrangement (Figure S2). For determination of the potential recognition regions and the catalytic residues of CLH10 for β-1,4-xyloside, each carboxylate residue involved in the alternative regions was mutated to alanine to construct single-site mutants. The mutants D10A and E139A abolished activity, while E53A and D203A retained 93.9% and 94.9% of the k_{cat}/K_m of the wild type, respectively (Figure 2), indicating that the recognition and catalytic region (I) was involved in the catalysis of CLH10 toward *p*NPX, and the residue pair composed of Asp10 and Glu139 was critical for hydrolyzing β-1,4-xyloside.

Additionally, to investigate the roles of Glu6, Asp136, and Asp135 in substrate recognition and catalysis, the kinetic parameters of mutants E6A, D136A, and D135A were measured (Figure 2). The k_{cat} of D136A (0.51 s^{-1}) was close to the k_{cat} of the wild type (0.53 s^{-1}), but the K_m of D136A (74.82 mM) was higher than that of the wild type (26.77 mM), indicating that Asp136 might be involved in the stabilization rather than substrate catalysis. Carboxylate residues (Asp and Glu) could stabilize the substrate through hydrogen bonding between its carboxyl group and the carbohydrate's hydroxyl group. However, Glu6 was not related to the stabilization of the substrate, because both k_{cat} and K_m of E6A were similar to those of the wild type. Interestingly, replacing Asp135 with Ala substantially enhanced the catalytic efficiency (k_{cat}/K_m) with both increased k_{cat} and decreased K_m; the replacement of Asp135 by Glu maintained almost the same catalytic efficiency as the wild type, and the mutation of Asp135 to Asn completely abolished the enzymatic activity. These results indicated that a longer side chain at position Asp135 restricted the binding of substrate, whereas a shorter side chain provided a larger space for the accommodation of substrate to accelerate substrate turnover, as demonstrated by the k_{cat} value. Meanwhile, both positively and negatively charged residues at the position of amino acid 135 could disturb the interaction between Asp136 and the substrate that delineated the affinity toward substrates, as demonstrated by K_m.

DOI: 10.1021/acscatal.8b03383
ACS Catal. 2019, 9, 1739−1747

Furthermore, the interaction plot between substrates and CLH10 suggested potential residues that involved in the recognition of acetyl ester or β-1,4-xyloside. These hypotheses were experimentally evaluated via site-directed mutagenesis. As shown in Figure 2, mutations of both Gly44 and Gly45 to Ala weakened the catalytic efficiency (k_{cat}/K_m) toward *p*NPA due to the decreased k_{cat} and lack of effect on K_m. The result suggested that Gly44 and Gly45 might act as the so-called "oxyanion hole" to stabilize the transition state of the substrate (Figure 3D). The oxyanion hole of serine esterase is formed by the N atoms of the critical residues (e.g., Gly, Asn, and Arg) and engages the oxyanion of the carbonyl group of the substrate via important hydrogen bonding interaction. On the other hand, two hydrogen bonds were observed between the xylose unit of *p*NPX and the two residues Trp5 and Arg89 (Figure 3C). These results indicated that the interactions of Trp5 and Arg89 with xyloside were important for substrate recognition. The mutant R89A retained 17.2% of the k_{cat}/K_m of the wild type because of a significant increase in K_m. The mutant W5A was inactive, but the activity was restored when the tryptophan residue was replaced with an alternative aromatic residue (Figure 2). This result indicated that the stacking interaction between Trp5 and the xyloside ring was essential for substrate binding.

3.4. Relationship of Two Functionalities. The relationship of the two functionalities of CLH10 was investigated from the perspectives of catalytic action, structural dynamics, and structural evolution. First, the catalytic activities of CLH10 toward acetyl ester bond and xylosidic bond were characterized in the unary-substrate system and dual-substrate systems. For avoidance of the effect of the hydrolysis products of *p*NPX and *p*NPA in the photometric assay, xylotetraose was employed as a substrate to characterize the catalytic activity toward the xylosidic bond. In the dual-substrate reaction system with the addition of both *p*NPA and xylotetraose, the activity toward *p*NPA was maintained, and the released reducing sugar contents were similar to those in the unary-substrate reaction system (Figure 4A). This result indicated that the catalytic roles of CLH10 in relation to the acetyl ester bond and xylosidic bond were independent of each other. According to the results of molecular docking (Table S6), the xylotetraose molecule docked in the pocket of the β-1,4-xylanase active region containing the residue range of Asn7−Leu13 and Asp136−Ser142, while the *p*NPA molecule docked in the pocket of the acetyl ester active region containing the residue range of Leu111−Gly117 (Figure 4B and Figure S3). Furthermore, the dynamic cross-correlation matrix (DCCM) showed that the residue region Leu111−Gly117 was unrelated to both the residue region Asn7−Leu13 and Asp136−Ser142 in the aspect of structural dynamics (Figure S4). For exploration of the structural evolution action between the esterase and glycoside hydrolase functionalities of CLH10, a structure similarity comparison was carried out using the DALI server.[30] From the Protein Data Bank, 20 structures with DALI *Z*-scores of higher than 24.5 were selected to construct the structural similarity dendrogram (Figure 4C and Table S7). The three known structures most closely related to CLH10 (PDB: 4BZW, 4Q3K, and 3HXK) were all described as α/β hydrolases in NCBI. Additionally, their sequences all encode the putative conserved domain of the acetyl esterase/lipase (Aes) superfamily detected by the CD-Search tool of NCBI.[31]

4. DISCUSSION

The enzymatic degradation of xylan is a widely used biomanufacturing strategy with prospective applications in food manufacturing, animal feed, and biofuel industries.[32] Xylan is a complex molecule to biodegrade due to the interaction between the main chain of β-(1,4)-linked D-xylopyranose and the heterogeneous side chains such as arabinose, acetyl ester, and feruloyl ester.[33] For efficient hydrolyzation of xylan, a series of different enzymes capable of cleaving off the main chain (xylosidase, etc.) and side chains (arabinosidase, acetylesterase, etc.) of xylose have been utilized together for effective synergistic degradation; however, the use of multiple enzymes led to a more difficult optimization process and higher cost in biotechnology engineering.[1] CLH10 isolated from *C. lactoaceticus* 6A, which grows well at temperatures from 50 to 78 °C and pH values from 5.8 to 8.2,[10] exhibited both acetyl esterase and β-1,4-xylanase activity and could simultaneously hydrolyze the main chain and acetylated side chain of xylan in a temperature range from 50 to 80 °C and pH from 6.0 to 8.0. The higher reaction temperature is advantageous in enzymatic applications, because it facilitates higher reactivity, higher process yield, lower viscosity, and lower microbial contamination.[34] Although the cleaving efficiency (k_{cat}/K_m) of CLH10 toward the β-1,4-xylosidic bond was not sufficient for the enzymatic degradation of xylan on an industrial scale, the substitution of Asp135 by Ala with improved activity exhibited potential for protein engineering to improve the β-1,4-xylanase activity of CLH10. Additionally, compared to previously reported AEXH, such as Xyn11A[35] and rPcAxe2,[36] CLH10 has a lower molecular weight, which could decrease its cost in biotechnology applications.

In the aspect of the primary sequence, most reported AEXHs contain two separated SRs, one of which encodes the CSE, and the other encodes the CSG (Figure 5A). For example, the sequence of AEXH from *Neocallimastix patriciarum* (XynS20E) includes the conserved domain of family 1 carbohydrate esterase at the N-terminus and the conserved domain of family 11 glycosyl hydrolase at the C-terminus.[37] The sequence of AEXH from *Pseudobutyrivibrio*

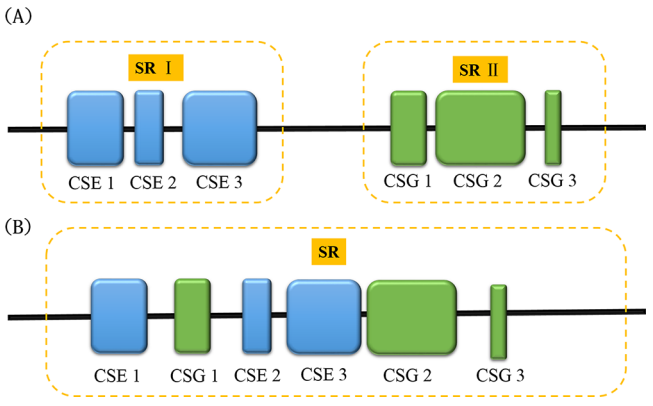

Figure 5. Schematic distribution of the conserved sequence of bifunctional acetyl ester−xyloside hydrolases. The conserved sequence of esterase (CSE) and the conserved sequence of glycosidase (CSG) are given in blue and green, respectively. (A) Bifunctional acetyl ester−xyloside hydrolase with two separate sequence regions (SRs). (B) Bifunctional acetyl ester−xyloside hydrolase with a single SR.

DOI: 10.1021/acscatal.8b03383
ACS Catal. 2019, 9, 1739−1747

xylanivorans Mz5^T (Xyn11A) encodes the acetyl xylan esterase domain NodB and the conserved domain of family 11 glycosyl hydrolases, and the domains are linked by the saccharide-binding module from family 6 (CBM6).[35] However, CLH10 is a rare single-SR bifunctional enzyme with CSG and CSE fragments distributing in a mixed type (Figure 5B). This special distribution pattern also exists in a bifunctional enzyme PcAxe.[38] However, the underlying dual-substrate recognition and catalytic mechanisms of this type of bifunctional enzyme are still unknown.

In the aspect of the three-dimensional structure, proteins often use multiple domains to perform tasks that require more than one function.[39] On the basis of the knowledge of bifunctional enzymes with two separated functional domains, a fusion protein strategy has been widely used to construct desired multifunctional enzymes by "end-to-end" or "insertional" modes at the genetic level.[2] However, CLH10 consists of a single structural domain, in which two different functionalities have evolved in two specific structure regions. There is no general principle to evolve a protein with a single domain by the mutation of several amino acids to achieve a novel enzyme function. The significance of loops for enzyme function and stability has been indicated, and the recognition of the potential of loops for catalysis is increasing.[39,40] Our work demonstrated advances in flexible loops for the generation of promising enzyme function. Both Asp10 and Glu139 are located in the loop region of CLH10. Loop regions are the most flexible parts of enzyme structures. Loops exposed on the surface often play a vital role in β-1,4-xylanase activity, because they have a greater opportunity to interact with the solvent and substrate molecules. The evolution of enzymes frequently involves their residue changes localized in the loop region.[39] Usually, enzymes are characterized by the conservation of their functional residues through evolution. However, both Asp10 and Glu139 are not conserved in CLH10 according to the analysis of the evolutionary conservation profile using the ConSurf server (Figure S5). The variable amino acids at the equivalent position of Asp10 and Glu139 located in the loop region and exposed on the surface might allow CLH10 to fortuitously generate hydrolytic activity toward the β-1,4-xylosidic bond. Furthermore, the structural evolution analysis by the DALI server indicated that CLH10 appeared to be an esterase that evolved glycoside hydrolase activity in the loop regions containing Asp10 and Glu139. Additionally, the crystal structure of apo-CLH10 revealed that a single SR could fold into two independent functional regions to perform acetyl esterase and β-1,4-xylanase hydrolysis functionalities, respectively (Figure 4D). Concerning catalytic bifunctionality, CLH10 belongs to neither the glycoside hydrolase nor carbohydrate esterase family in the Carbohydrate Active Enzymes Database (CAZY).[41] In the future work, deeper insight into the proton transfer mechanisms between catalytic residues and substrate should be investigated through the studies of the enzyme−substrate crystal structures or quantum mechanics/molecular mechanics (QM/MM) molecular dynamics simulations. In summary, our findings paved an alternative way to evolve promising enzyme function in proteins with a single domain by acting on the loop region, both in directed evolution and in rational protein engineering.

■ ASSOCIATED CONTENT

Supporting Information

The Supporting Information is available free of charge on the ACS Publications website at DOI: 10.1021/acscatal.8b03383.

Primers used for site-directed mutagenesis; data collection and refinement statistics of crystal structure; molecular docking results; structure comparison analysis by DALI server; purification characterization; LigPlot 2D diagram; per-residue dynamic cross-correlation matrix; and conservation pattern of residues (PDF)

■ AUTHOR INFORMATION

Corresponding Authors

*E-mail: wangfengzhong@sina.com.
*E-mail: 2002hongzhi30@163.com.

ORCID

Hao Cao: 0000-0002-5118-6664
Lichao Sun: 0000-0002-3621-5252

Author Contributions

$^{\nabla}$H.C. and L.S. contributed equally to this article.

Notes

The authors declare no competing financial interest.

■ ACKNOWLEDGMENTS

We thank Prof. Yejun Han for kindly offering the plasmid. We also thank the Shanghai Synchrotron Radiation Facility (SSRF) for beam time allocation and data collection assistance. This work was supported by the National Key Research and Development Plan "modern food processing and food storage and transportation technology and equipment" (2017YFD0400204), China Postdoctoral Science Foundation (2018M630230), and National Natural Science Foundation of China (31801475 and 31700701).

■ REFERENCES

(1) Liu, X.; Shi, P. J.; Yang, P. L.; Yao, B. Research Progress on Bifunctional Xylanases. *J. Agric. Sci. Technol.* **2010**, *12*, 50−56.
(2) Khandeparker, R.; Numan, M. T. Bifunctional Xylanases and Their Potential Use in Biotechnology. *J. Ind. Microbiol. Biotechnol.* **2008**, *35*, 635−644.
(3) Chen, H. G.; Yan, X.; Liu, X. Y.; Wang, M. D.; Huang, H. M.; Jia, X. C.; Wang, J. A. Purification and Characterization of Novel Bifunctional Xylanase, XynIII, Isolated from *Aspergillus niger* A-25. *J. Microbiol. Biotechnol.* **2006**, *16*, 1132−1138.
(4) Numan, M. T.; Bhosle, N. B. α-L-Arabinofuranosidases: the Potential Applications in Biotechnology. *J. Ind. Microbiol. Biotechnol.* **2006**, *33*, 247−260.
(5) Xie, G.; Bruce, D. C.; Challacombe, J. F.; Chertkov, O.; Detter, J. C.; Gilna, P.; Han, C. S.; Lucas, S.; Misra, M.; Myers, G. L. Genome Sequence of the Cellulolytic Gliding Bacterium Cytophaga hutchinsonii. *Appl. Environ. Microbiol.* **2007**, *73*, 3536−3546.
(6) Selig, M. J.; Knoshaug, E. P.; Adney, W. S.; Himmel, M. E.; Decker, S. R. Synergistic Enhancement of Cellobiohydrolase Performance on Pretreated Corn Stover by Addition of Xylanase and Esterase Activities. *Bioresour. Technol.* **2008**, *99*, 4997−5005.
(7) Zhang, J.; Siika-Aho, M.; Tenkanen, M.; Viikari, L. The Role of Acetyl Xylan Esterase in the Solubilization of Xylan and Enzymatic Hydrolysis of Wheat Straw and Giant Reed. *Biotechnol. Biofuels* **2011**, *4*, 60.
(8) Stok, J. E.; Goloshchapov, A.; Song, C.; Wheelock, C. E.; Derbel, M. B.; Morisseau, C.; Hammock, B. D. Investigation of the Role of a Second Conserved Serine in Carboxylesterases via Site-directed Mutagenesis. *Arch. Biochem. Biophys.* **2015**, *430*, 247−255.

DOI: 10.1021/acscatal.8b03383
ACS Catal. 2019, 9, 1739−1747

(9) Bourne, Y.; Henrissat, B. Glycoside Hydrolases and Glycosyltransferases: Families and Functional Modules. *Curr. Opin. Struct. Biol.* **2001**, *11*, 593−600.
(10) Mladenovska, Z.; Mathrani, I. M.; Ahring, B. K. Isolation and Characterization of *Caldicellulosiruptor lactoaceticus* sp. nov., an Extremely Thermophilic, Cellulolytic, Anaerobic Bacterium. *Arch. Microbiol.* **1995**, *163*, 223−230.
(11) Liu, X.; Liu, T.; Zhang, Y.; Xin, F.; Mi, S.; Wen, B.; Gu, T.; Shi, X.; Wang, F.; Sun, L. Structural Insights into the Thermophilic Adaption Mechanism of Endo-1,4-*β*-Xylanase from *Caldicellulosiruptor owensensis*. *J. Agric. Food Chem.* **2018**, *66*, 187.
(12) Otwinowski, Z.; Minor, W. Processing of X-ray Diffraction Data Collected in Oscillation mode. *Methods Enzymol.* **1997**, *276*, 307−326.
(13) Langer, G.; Cohen, S. X.; Lamzin, V. S.; Perrakis, A. Automated Macromolecular Model Building for X-ray Crystallography using ARP/wARP version 7. *Nat. Protoc.* **2008**, *3*, 1171−1179.
(14) Nonaka, T. The CCP 4 Suite: Programs for Protein Crystallography. *Acta Crystallogr., Sect. D: Biol. Crystallogr.* **1994**, *50*, 760−763.
(15) Adams, P. D.; Grossekunstleve, R. W.; Hung, L. W.; Ioerger, T. R.; Mccoy, A. J.; Moriarty, N. W.; Read, R. J.; Sacchettini, J. C.; Sauter, N. K.; Terwilliger, T. C. PHENIX: Building New Software for Automated Crystallographic Structure Determination. *Acta Crystallogr., Sect. D: Biol. Crystallogr.* **2002**, *58*, 1948−1954.
(16) Emsley, P.; Cowtan, K. Coot: Model-Building Tools for Molecular Graphics. *Acta Crystallogr., Sect. D: Biol. Crystallogr.* **2004**, *60*, 2126−2132.
(17) Berman, H. M.; Westbrook, J.; Feng, Z.; Gilliland, G.; Bhat, T. N.; Weissig, H.; Shindyalov, I. N.; Bourne, P. E. The Protein Data Bank. *Genetica* **2000**, *106*, 149−158.
(18) Breuil, C.; Saddler, J. N. Comparison of the 3,5-Dinitrosalicylic Acid and Nelson-Somogyi Methods of Assaying for Reducing Sugars and Determining Cellulase Activity. *Enzyme Microb. Technol.* **1985**, *7*, 327−332.
(19) Ashkenazy, H.; Abadi, S.; Martz, E.; Chay, O.; Mayrose, I.; Pupko, T.; Bental, N. ConSurf 2016: An Improved Methodology to Estimate and Visualize Evolutionary Conservation in Macromolecules. *Nucleic Acids Res.* **2016**, *44*, W344−W350.
(20) Celniker, G.; Nimrod, G.; Ashkenazy, H.; Glaser, F.; Martz, E.; Mayrose, I.; Pupko, T.; BenTal, N. ConSurf: Using Evolutionary Data to Raise Testable Hypotheses about Protein Function. *Isr. J. Chem.* **2013**, *53*, 199−206.
(21) Ashkenazy, H.; Erez, E.; Martz, E.; Pupko, T.; Bental, N. ConSurf 2010: Calculating Evolutionary Conservation in Sequence and Structure of Proteins and Nucleic Acids. *Nucleic Acids Res.* **2010**, *38*, 529−533.
(22) Lobo, I. Basic Local Alignment Search Tool (BLAST). *J. Mol. Biol.* **1990**, *215*, 403−410.
(23) Trott, O.; Olson, A. J. AutoDock Vina: Improving the Speed and Accuracy of Docking with a New Scoring Function, Efficient Optimization, and Multithreading. *J. Comput. Chem.* **2009**, *31*, 455−461.
(24) Krieger, E.; Vriend, G. YASARA View-Molecular Graphics for All Devices from Smartphones to Workstations. *Bioinformatics* **2014**, *30*, 2981−2982.
(25) Stewart, J. J. MOPAC: a Semiempirical Molecular Orbital Program. *J. Comput.-Aided Mol. Des.* **1990**, *4*, 1−105.
(26) Delano, W. L. *PyMOL Molecular Graphics System*; Schrödinger, 2002.
(27) Krieger, E.; Vriend, G. New Ways to Boost Molecular Dynamics Simulations. *J. Comput. Chem.* **2015**, *36*, 996−1007.
(28) Piana, S.; Lindorff-Larsen, K.; Shaw, D. E. How Robust are Protein Folding Simulations with Respect to Force Field Parameterization? *Biophys. J.* **2011**, *100*, L47−L49.
(29) Blow, D. M.; Birktoft, J. J.; Hartley, B. S. Role of a Buried Acid Group in the Mechanism of Action of Chymotrypsin. *Nature* **1969**, *221*, 337−340.
(30) Holm, L.; Rosenström, P. Dali server: Conservation Mapping in 3D. *Nucleic Acids Res.* **2010**, *38*, W545−W549.
(31) Marchler-Bauer, A.; Bo, Y.; Han, L.; He, J.; Lanczycki, C. J.; Lu, S.; Chitsaz, F.; Derbyshire, M. K.; Geer, R. C.; Gonzales, N. R. CDD/SPARCLE: functional classification of proteins via subfamily domain architectures. *Nucleic Acids Res.* **2017**, *45*, D200−D203.
(32) Naidu, D. S.; Hlangothi, S. P.; John, M. J. Bio-based Products from Xylan: A Review. *Carbohydr. Polym.* **2018**, *179*, 28.
(33) Petzold-Welcke, K.; Schwikal, K.; Daus, S.; Heinze, T. Xylan Derivatives and Their Application Potential Mini-review of Own Results. *Carbohydr. Polym.* **2014**, *100*, 80−88.
(34) Collins, T.; Gerday, C.; Feller, G. Xylanases, Xylanase Families and Extremophilic Xylanases. *FEMS Microbiol. Rev.* **2005**, *29*, 3.
(35) Cepeljnik, T.; Rincón, M. T.; Flint, H. J.; Marinseklogar, R. Xyn11A, a Multidomain Multicatalytic Enzyme from *Pseudobutyrivibrio xylanivorans* Mz5T. *Folia Microbiol.* **2006**, *51*, 263.
(36) Huy, N. D.; Thiyagarajan, S.; Kim, D. H.; Park, S. M. Cloning and Characterization of A Novel Bifunctional Acetyl Xylan Esterase with Carbohydrate Binding Module from *Phanerochaete chrysosporium*. *J. Biosci. Bioeng.* **2013**, *115*, 507.
(37) Pai, C. K.; Wu, Z. Y.; Chen, M. J.; Zeng, Y. F.; Chen, J. W.; Duan, C. H.; Li, M. L.; Liu, J. R. Molecular Cloning and Characterization of a Bifunctional Xylanolytic Enzyme from *Neocallimastix patriciarum*. *Appl. Microbiol. Biotechnol.* **2010**, *85*, 1451−1462.
(38) Yang, Y.; Zhu, N.; Yang, J.; Lin, Y.; Liu, J.; Wang, R.; Wang, F.; Yuan, H. A Novel Bifunctional Acetyl Xylan Esterase/Arabinofuranosidase from *Penicillium chrysogenum* P33 Enhances Enzymatic Hydrolysis of Lignocellulose. *Microb. Cell Fact.* **2017**, *16*, 166.
(39) Nestl, B. M.; Hauer, B. Engineering of Flexible Loops in Enzymes. *ACS Catal.* **2014**, *4*, 3201−3211.
(40) Saavedra, H. G.; Wrabl, J. O.; Anderson, J. A.; Li, J.; Hilser, V. J. Dynamic Allostery Can Drive Cold Adaptation in Enzymes. *Nature* **2018**, *558*, 324−328.
(41) Lombard, V.; Golaconda, R. H.; Drula, E.; Coutinho, P. M.; Henrissat, B. The Carbohydrate Active Enzymes Database (CAZy) in 2013. *Nucleic Acids Res.* **2014**, *42*, D490.

DOI: 10.1021/acscatal.8b03383
ACS Catal. 2019, 9, 1739−1747